Magmatic Processes: Physicochemical Principles
© The Geochemical Society, Special Publication No. 1, 1987
Editor B. O. Mysen

The petrogenetic role of methane: Effect on liquidus phase relations and the solubility mechanism of reduced C–H volatiles

W. R. TAYLOR and D. H. GREEN
Geology Department, University of Tasmania, GPO Box 252C, Hobart, Australia 7001

Abstract—Methane and other reduced volatiles may be an important species in the Earth's mantle. The nature of mantle partial melting under reduced conditions in the presence of such volatiles is, however, largely unknown. To evaluate the petrogenetic role of C–H volatiles experimental liquidus studies were undertaken in the system nepheline(Ne)–forsterite(Fo)–silica(Q)–C–O–H at 28 kbar. Methane-dominated fluids are conveniently generated in high pressure experiments from a mixture of Al_4C_3 and $Al(OH)_3$. Compared to the volatile–absent system, the effect of CH_4–rich fluids is to expand the Fo phase field relative to En_{ss} (melt depolymerization) and to bring phases of high octahedral aluminum content onto the liquidus (leading to early appearance of garnet on the liquidus of other compositions). This contrasts with the effect of CO_2 which gives rise to the expansion of the En_{ss} phase field and the effect of H_2O which results in a greater expansion of the Fo field than CH_4. The magnitude of liquidus temperature depressions for C–H fluid–saturated Fo–Ne–Q melts are comparable to that of pure CO_2 (~90°C at 28 kbar).

Infrared (IR) spectroscopic investigations of C–H fluid saturated jadeite and sodamelilite glasses quenched from 30 kbar, establish the presence of both dissolved, oxidized, and reduced components as also required by charge-balance constraints. The former occurs as O–H groups and the latter is consistent with a reduced network component of O:Si stoichiometry <2 ("silicon monoxide" units). There is no spectroscopic evidence for the presence of dissolved molecular CH_4, other C–H groups or carbonate. Pyrolysis/gas chromatographic analyses give dissolved H contents equivalent to ~3 weight percent H_2O and reduced C contents of 1000–2000 ppm (wt) in a form yet to be characterized. Aluminosilicate melts have a strong preference for dissolved H over C under reduced conditions.

INTRODUCTION

MAJOR ADVANCES in understanding the role of volatile components in igneous petrogenesis have taken place over the last ten years. Much of this effort has been directed at determining the petrogenetic role of the oxidized volatiles CO_2 and H_2O which are known to have a significant effect on super-solidus phase relations at upper mantle pressures (see review by HOLLOWAY, 1981).

Because H_2O and CO_2 are the most abundant species in volcanic gases (*e.g.*, ANDERSON, 1975), it has been commonly assumed that they will also be the most abundant species at depth in the Earth's upper mantle. If this basic assumption is incorrect, and this will depend to a large extent on the mantle's oxidation state, then the role of volatiles other than H_2O and CO_2 must be considered (RYABCHIKOV *et al.*, 1981).

A variety of evidence exists to support the idea that at least part of the upper mantle is reduced enough to stabilize CH_4 at depth ($f_{O_2} \leq$ IW + 2 log units). This evidence includes intrinsic oxygen fugacity measurements on mantle-derived minerals indicating the prevalence of low f_{O_2} conditions amongst "type A" upper mantle (ARCULUS and DELANO, 1981) and the finding of primordial (^{3}He correlated) CH_4 as a significant component of fluids outgassing at mid-ocean ridge hydrothermal centers (WELHAN and CRAIG, 1981, 1983). Current views on the redox state of the Earth's mantle have recently been summarized by WOERMANN and ROSENHAUER (1985, in particular see pp. 317–322). Although this area is still one of active debate and inquiry, it seems likely that a range of oxidation states from relatively oxidized ($f_{O_2} \sim$ FMQ) to reduced ($f_{O_2} \sim$ IW) are applicable to the upper mantle. Volatiles in the reduced part of the system C–O–H may therefore be of considerable importance in igneous petrogenesis.

If magma generation involving volatile components takes place in a reduced environment, for example at f_{O_2}'s near the iron-wustite (IW) oxygen buffer, then in the model system "peridotite"–C–O–H, volatiles will be dominantly $CH_4 > H_2O > H_2 > C_2H_6$ mixtures and crystalline carbonates will not be stable relative to diamond or graphite (RYABCHIKOV *et al.*, 1982; EGGLER and BAKER, 1982). To explore the nature of mantle melting under reduced conditions an adequate understanding of the thermodynamic properties of C–O–H fluids at elevated pressures and temperatures is required. Reduced volatile interactions with silicate melts can then be investigated by experimental and spectroscopic means. The first aspect has been considered by TAYLOR (1985, 1987) and the second is the purpose of this paper.

The contrasting effects of oxidized versus reduced volatiles on liquidus phase relations are investigated in the model peridotite system nepheline(Ne)–forsterite(Fo)–silica(Q) under conditions of CH_4, CO_2 and H_2O volatile saturation and in the absence of volatiles. To place constraints on the mechanism of reduced C–H volatile dissolution in aluminosilicate melts, CH_4-saturated, graphite-free glasses of sodamelilite ($NaCaAlSi_2O_7$, Sm) and jadeite ($NaAlSi_2O_6$, Jd) composition have been analysed for carbon and hydrogen and investigated by Fourier Transform infrared (FTIR) spectroscopic methods.

Iron–bearing compositions have not been considered in this study primarily because f_{O_2} conditions in the presence of a C–H fluid will lie well within the Fe-metal stability field. The effect of reduced volatiles on these compositions must instead be investigated in the presence of mixed H_2O–CH_4–H_2 fluids at higher f_{O_2}'s (near the IW buffer for example). In this study we concentrate on identifying the mechanism of reduced C–H volatile dissolution free from interference by other species and thus provide the necessary basis for extension into natural systems.

PREVIOUS WORK ON REDUCED C–H VOLATILE INTERACTIONS WITH SILICATE MELTS

Little is known of how reduced volatiles interact with silicate melts. EGGLER and BAKER (1982) conducted a number of reconnaissance experiments determining the effect of C–H volatiles on the melting and liquidus phase relations of diopside and the composition diopside $(Di)_{35}$ pyrope $(Py)_{65}$ at $P > 20$ kbar. Experimental f_{O_2} conditions were believed to be near the Si–SiO_2 buffer but could not be determined directly. EGGLER and BAKER (1982) found liquidus depressions of ~100°C in diopside at 21 kbar and a large liquidus field of olivine plus garnet extending to at least 40 kbar in $Di_{35}Py_{65}$ coexisting with C–H fluid. In the latter case this differs from the effect of H_2O which does not bring garnet onto the liquidus and the effect of CO_2 which stabilizes orthopyroxene to high pressures. The presence of "depolymerized" phases such as olivine and garnet on the C–H volatile saturated liquidus led to the suggestion that reduced volatiles have a depolymerizing effect on silicate melts. Quench problems did not allow spectroscopic investigation of the glasses produced in their study and a detailed solubility mechanism could not be ascertained. In the only other study involving CH_4–bearing fluids, JAKOBSSON (1984), using a pyrolysis/mass spectrometry technique, determined the dissolved volatile content of quenched albite glasses equilibrated with H_2O–CH_4 fluids at 10–25 kbar (f_{O_2} ~ IW). Gases released at 1200°C consisted mainly of H_2O (>80 mol percent) with smaller amounts of reduced volatiles (CO, CH_4 and H_2). The extent to which dispersed graphite in the samples affected results was not assessed; low total C/H ratios (<0.06), however, suggest reduced carbon solubilities are not large under these conditions. Raman and infrared (IR) spectroscopic measurements confirmed the dominance of dissolved water; carbonate and possibly molecular methane were detected in some samples. Recently, LUTH and BOETTCHER (1986) have demonstrated that H_2, a significant component of C–H fluids at high pressures, interacts strongly with silicate liquids and may be quite soluble in silicate melts.

In the light of the above studies it is of importance to establish the nature and mechanism of reduced C–H volatile interaction with silicate systems. Problems of graphite contamination, quench effects and uncertainty in the nature of the C–H fluids actually generated have limited previous studies. Resolution of these problems is essential for obtaining unambiguous spectroscopic and analytical results. The f_{O_2} conditions chosen for the present study are such that CH_4 is the dominant fluid species. At higher f_{O_2}'s, where H_2O becomes important, the effects of reduced C–H volatiles may not be clearly resolved from those of H_2O.

EXPERIMENTAL TECHNIQUES

High pressure experiments

All high pressure experiments were performed with 0.5″–diameter (1.27 cm) solid-media, high-pressure apparatus using techniques similar to those of GREEN and RINGWOOD (1967). Temperatures were recorded with a Pt/$Pt_{90}Rh_{10}$ thermocouple automatically controlled to within ±5–7°C of the set value. All experiments were carried out by using the "piston-in" technique and applying a −10% pressure correction to nominal load pressures; quoted pressures are accurate to ±1 kbar.

Silicate compositions in the system nepheline–forsterite–silica (Ne–Fo–Q) were prepared from analytical reagent grade Al_2O_3, SiO_2, Na_2CO_3 and MgO fired at 900°C after thorough mixing and repeated grinding under acetone. Compositions were checked by microprobe analysis of glass beads prepared from the sintered oxide mixes on an Ir–strip heater. Sodamelilite and jadeite starting materials were powdered glasses prepared from sintered oxides. Samples were melted at 1250°C in Pt–crucibles and quenched in air to colorless glasses; their composition and homogeneity were checked by microprobe analysis.

Methane-saturated experiments

Calculations by TAYLOR (1985, 1987) reveal that under upper mantle pressure-temperature conditions C–H fluids in equilibrium with graphite contain CH_4 as a major (>80 mol percent) component and H_2 and C_2H_6 as minor (<10 mol percent) components. Such fluids are stable only at f_{O_2}'s below ~IW–4 log f_{O_2} units. Under these conditions f_{H_2} is large so that maintenance of fluid excess conditions during an experiment requires minimization of diffusive H_2-loss by employing run durations as short as possible while still achieving fluid–melt equilibrium. In preliminary studies, we found that the use of complex organic compounds as a methane-source (such as those used by HOLLOWAY and REESE, 1974; EGGLER and BAKER, 1982) results in the formation of disordered graphite which persists in experiments for run durations of less than a few hours. To overcome this problem in short duration experiments that do not incorporate a solid f_{O_2} buffer (as those undertaken here), methane should ideally be produced rapidly and by direct reaction.

Methane, together with a small amount of H_2, can be readily generated at 1 bar by the action of H_2O on Al_4C_3 (WADE and BANISTER, 1973). Because this reaction proceeds rapidly to completion and produces a C–H fluid with a CH_4:H_2 ratio of ~9:1 (similar to that calculated for high pressure-temperature equilibrium), it is an ideally suited generation reaction. By including $Al(OH)_3$ as the source of H_2O a convenient solid reactant can be prepared. Overall the methane generation reaction may be written:

$$4Al(OH)_3 + Al_4C_3 \rightarrow 4Al_2O_3 + 3CH_4 (+H_2 + C_2H_6). \quad (1)$$

To give the fluid-generating carbide/hydroxide mixture sufficient bulk, alumina was used as a diluant giving a mixture capable of generating 0.2 mg CH_4/10 mg mix. To eliminate the possibility that adsorbed water or excess air in the capsule might lead to oxidation of methane and production of H_2O, a 1:1 molar ratio of $Al(OH)_3$ to Al_4C_3 (three times carbide excess over reaction stoichiometry) was employed. The presence of excess carbide was confirmed optically and by x-ray diffraction at the end of each experiment. All mixtures containing Al_4C_3 (98 weight percent purity, Goodfellows Metals #AL516010) were stored under vacuum desiccation to prevent reaction with atmospheric moisture.

Experiments with C–H volatiles were carried out in large capacity "buffer" assemblies using Pt outer capsules (3.5 mm O.D.) and inner unsealed Pt capsules containing ~15 mg of silicate sample. Sample–containing capsules were heated briefly to red-heat prior to loading the methane-source to ensure removal of all traces of adsorbed water. The inner capsule was surrounded with sufficient fluid–generating mix to produce ~1 mg of methane. For jadeite and sodamelilite compositions, experiments were of 30 minutes duration at 30 kbar, 1320°C and 1350°C, respectively; run details for system Ne–Fo–Q experiments are listed in the Appendix. Talc was chosen as the pressure transmitting medium to maximize the external f_{H_2} of the system and thus limit H_2 loss from the capsule.

Prior to experiments with silicates a "blank" run was performed at 30 kbar, 1300°C for 15 minutes with the aim of determining whether fluid phase equilibrium is achievable in short run times by this technique. Analysis of the fluid phase following the run was accomplished by mass spectrometry using a capsule piercing technique. The presence of a vapor phase is readily recognized by the distended nature of the capsule. The device used for capsule piercing consists of a modified regulating valve (Whitey #SS–1VS6) with a redesigned stem tip fashioned into a hardened needle point. A removable cradle serves to position and hold the capsule in place during piercing. Gases were released under vacuum (~10^{-6} torr) and directed into the ion-source of a VG–micromass 7070 double focusing mass spectrometer via a modified probe insertion technique. To achieve low background levels, particularly for H_2O caused chiefly by absorbed molecules on metal surfaces, it was found necessary to evacuate the whole system (probe plus piercer) for ~12 hours prior to taking measurements. After piercing, mass spectra were acquired by multiple scans of ~2 sec duration over the mass range 10–70 m/z. The total ion current was monitored during the piercing experiment and both background and sample spectra were recorded at various sensitivities. With the data acquisition system used by the VG instrument, H_2 was below the lower mass–range limit of recorded spectra. The presence of both H^+ and H_2^+ ions was, however, confirmed qualitatively by oscillographic traces down to low mass numbers. Mass spectra are normalized to zero background (mainly residual air and water vapor in the instrument) by reference to the m/z 32 (O_2^+) or 40 (Ar^+) peak. X–ray diffraction (XRD) and optical examination of the solid product showed the presence of Al_2O_3, ordered graphite and excess Al_4C_3. No oxycarbides were identified either optically or by XRD. The presence of abundant ordered graphite indicates that an f_{H_2} buffer reaction of the type: C(graphite) + $2H_2$ = CH_4, has been operative during the experiment. The form of the mass spectra for the blank experiment and for those experiments with silicate present are identical except a finite amount of H_2O (<0.2 mol percent) is found in the latter. Figure 1 shows a typical methane (m/z 12–16) and ethane (m/z 24–30, m/z 28 overlaps with background N_2^+) spectrum for an experiment with silicate present. Trace amounts of C_{3-4} hydrocarbons are also present. Although the C_2H_6/CH_4 ratio of the fluid is slightly higher than predicted by the MRK–equation calculations of TAYLOR (1986): ~25 vs. 18 expected, overall the agreement with theory is good. Derived fluids are thus believed to represent those at graphite-fluid equilibrium. The absence of oxygen–containing volatiles (*i.e.*, H_2O) places an upper limit on the $\log f_{O_2}$ of the system at near IW–5 $\log f_{O_2}$ units under experimental conditions for the "blank" experiments and near IW–4.5 $\log f_{O_2}$ units for those containing silicate. The use of a carbide/hydroxide mixture is thus a rapid and convenient method for preparing fluids dominated by CH_4 at high pressures.

Water, carbon dioxide and volatile–absent experiments

These experiments were performed in talc/pyrex or talc–only (for water–saturated runs) sleeved assemblies using 2.3 mm O.D. Pt or $Ag_{50}Pd_{50}$ capsules. H_2O (~30 weight percent) was added via microsyringe and CO_2 (~15 weight percent) was generated from $Ag_2C_2O_4$. Run times for CO_2 and volatile–absent experiments were kept to <20 min. (see Appendix) to avoid the risk of H_2O formation by hydrogen diffusion into the capsule. All mixes and assembly parts were dried at 120°C, 24 hours prior to use.

Spectroscopic methods

Spectra of C–H fluid—saturated glasses were investigated by Fourier Transform infrared (FTIR) spectroscopy using a Digilab model FTS–20E spectrometer. FTIR spectroscopy offers significant advantages over conventional instrumentation, including increased signal–to–noise ratio, increased sensitivity due to high energy throughput and ready access to computer-based data manipulation procedures such as band fitting and spectrum subtraction. Spectra of both powdered glass and crystalline samples were obtained by the conventional KBr disc method. Aproximately 2 mg (1 mg for crystalline compounds) of sample was ground together with 200 mg of IR–grade KBr in an agate mortar for 10 minutes. After drying the powder at 120°C, pellets were pressed between 1 cm diameter polished stainless steel dies; any cloudy discs were remade. Discs were then dried under P_2O_5 desiccant overnight to remove traces of adsorbed water. Spectra were acquired by signal averaging 200 scans at 4 cm^{-1} resolution referenced against a blank KBr disc.

Difficulties with KBr powder spectroscopy rest largely with its reproducibility. Differences in sample preparation, reflected mainly in particle size distribution and orientation effects may lead to changes in bandwidths and relative

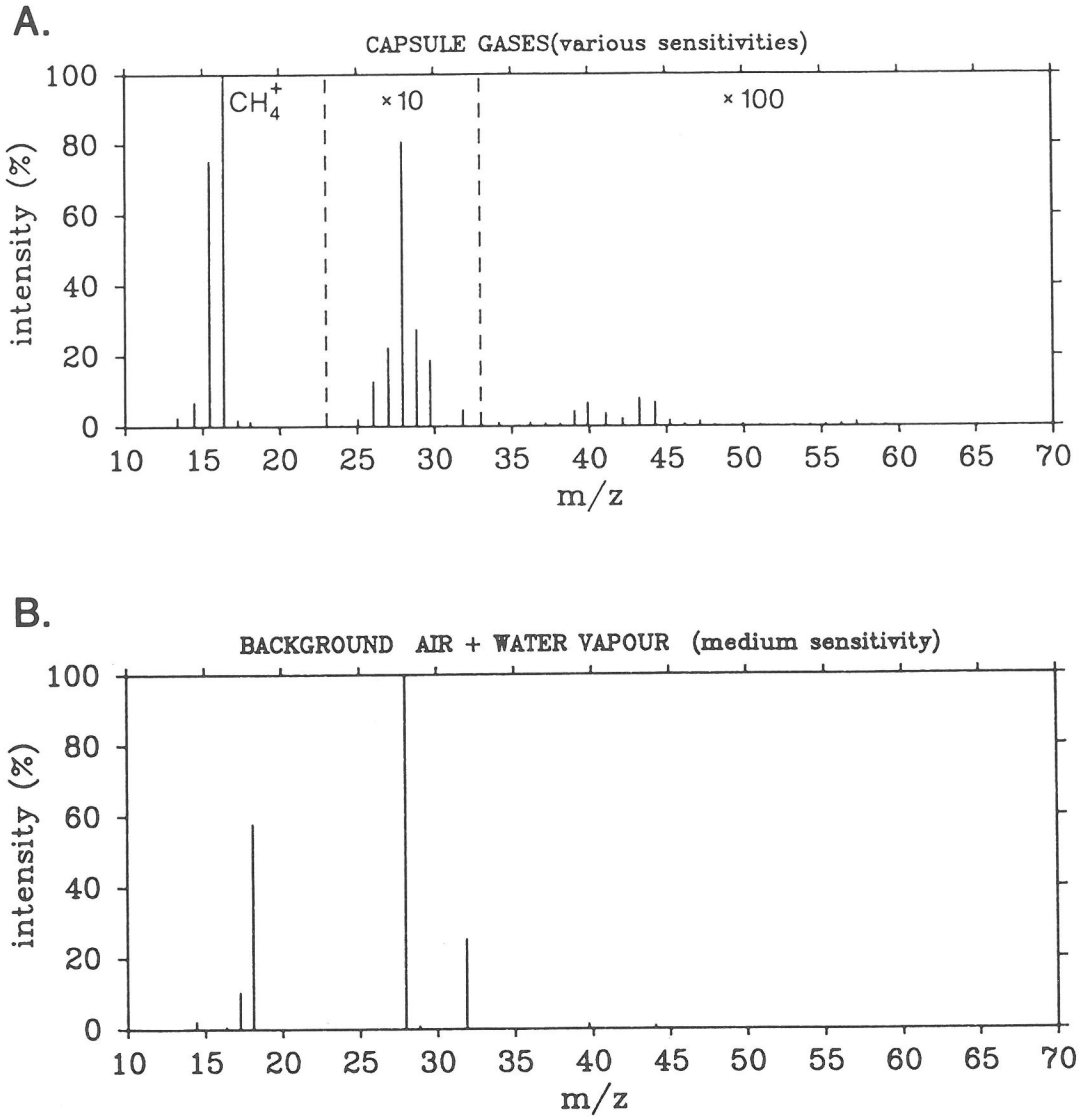

FIG. 1. (A) Mass spectrum of capsule gases released from run T–1341 at low (m/z 10–23), medium (×10, m/z 23–33) and high (×100, m/z >33) sensitivities. Methane: m/z 13–17; ethane: m/z 25–30; C_{3-4} hydrocarbons m/z >36; background water vapour and air: m/z 17–18, 28, 32. (B) Instrumental background at medium sensitivity. Note suppression of background ion intensity due to input of capsule gases (ratios of individual gases, however, remain unchanged).

intensities (MCMILLAN, 1985). Such changes are of critical importance in quantitative studies but are of lesser importance in the interpretative work undertaken here. Nevertheless, reproducibility checks were performed by the preparation of duplicate discs, in all cases using identical preparative methods. Duplicates showed close similarity in spectral features (as illustrated in Figures 7A and 7B). It is believed that the reproducibility of the KBr disc method, provided sample preparation techniques remain consistent, is not a problem in the interpretation of the silicate glass and crystal spectra considered here.

Analytical Methods

Pyrolysis/gas chromatography

Quantitative carbon and hydrogen analyses of the C–H fluid–saturated glasses were performed with a Hewlett–Packard 185B CHN analyser at the Analytical Services Section, Research School of Chemistry, Australian National University). The method has been previously applied by BREY (1976) in the analysis of ~mg quantities of silicate glasses containing dissolved carbonate and water. For

C–H fluid–saturated glasses that may contain dissolved reduced components, ~0.5 to 1.5 mg of sample was intimately mixed with 85 mg of $MnO_2/WO_3/Cr_2O_3$ oxidant. Samples were then combusted at 1080°C for 90 seconds following an initial heating at 70°C to remove atmospheric gases.

In the pyrolysis of reduced C–bearing glasses, the possibility exists that crystallites of silicon carbide might form during the combustion process and remain unreactive to oxidation (SiC being known for its chemical inertness and high thermal stability: ROCHOW, 1973). To determine whether the pyrolysis/gas chromatography technique gives accurate results for the analysis of substances containing (or with the potential to form) Si–C bonds, three standard compounds consisting of mixtures of finely ground SiC and silica powder were analysed. Results for unknowns and standards are listed in Table 1. Standards were combusted for 90 seconds and 120 seconds (in the latter case there was a considerable loss in sensitivity).

Electron microprobe

Electron microprobe analyses for carbon were performed at the Electron Optical Centre (E.O.C.), University of Adelaide (JEOL 733 microprobe, B. J. Griffin analyst) and Central Science Laboratory, University of Tasmania (JEOL JXA50A microprobe). Measurements were obtained with a light element (STE crystal) wavelength dispersive spectrometer using 15 kV accelerating voltage in the former case and 10 kV in the latter. The beam in both cases was defocussed to a 10–20 μm diameter spot with 50 nA beam current to minimize specimen damage. Polished epoxy mounts containing the samples, blanks and an array of carbon standards (graphite, SiC and various carbonates) were coated with aluminum following the method of MATHEZ and DELANEY (1981). Analyses at E. O. C., Adelaide, were performed by 60 second counts on the peak and 20 seconds on the backgrounds with the spectrometer positioned 10 mm either side of the peak position. Full ZAF corrections were applied. Surface carbon contamination, derived from cracking of vacuum pump oils under the beam, resulted in a detection limit for carbon of ~0.2 weight percent. Analyses of standards, blanks and unknowns gave results of high consistency mainly due to the good precision obtainable with long counting times at reasonably high count rates. Absolute accuracy is difficult to judge due to the large matrix corrections used and the effects of surface contamination. These uncertainties could amount to errors of as much as ±30%.

Table 1. Pyrolysis/gas chromatography analytical results*

Sample #	Comp.	C (Weight percent)	H_2O (Weight percent)	Combustion time (sec)
T–1296	Jd	0.13 ± 0.03	2.9 ± 0.4	90
T–1341	Sm	0.09 ± 0.07	3.0 ± 0.5	90
T–1318	Sm	0.12 ± 0.04	1.7 ± 0.1	90
T–1250	Sm	not analysed	5.5 ± 0.2	90

Standards (SiC + SiO_2)	Actual weight percent C	Analysed weight percent C	Combustion time (sec)
A	0.5	0.24 ± 0.04	90
		0.18 ± 0.02	120
B	1.0	0.32 ± 0.03	90
		0.21 ± 0.06	120
C	1.5	0.51 ± 0.07	90

* All samples analysed in duplicate, averages and std deviations quoted.

Detection limits: C 0.05 weight percent; H as H_2O 0.18 weight percent.

CONTRASTING LIQUIDUS PHASE RELATIONS IN THE SYSTEM Ne–Fo–Q–C–O–H

At pressures >25 kbar the system nepheline(Ne)–forsterite(Fo)–silica(Q) contains liquidus phase fields of forsterite (Fo), enstatite$_{ss}$ (En_{ss}) and jadeite$_{ss}$ (Jd_{ss}) analogous to the major minerals of upper mantle peridotite. This system forms the base of the simplified basalt tetrahedron (YODER and TILLEY, 1962) and as such offers a useful model for investigating small degrees of partial melting of mantle peridotite. Liquidus phase relationships in the system Ne–Fo–Q have therefore been widely studied particularly as a function of pressure and activity of volatile species (KUSHIRO, 1968, 1972; EGGLER, 1978; WINDOM and BOETTCHER, 1981). The position of the Fo–En_{ss} two–phase boundary can be used as an indicator of melt–phase silica activity reflecting the relative degree of silicate melt polymerization/depolymerization (as discussed most recently by RYERSON, 1985). The aim of this study is to locate the Fo–En_{ss} two–phase boundary in the system Ne–Fo–Q under conditions dominated by a CH_4–rich vapor phase. Comparisons can then be made with the boundary position under volatile–absent, H_2O–saturated and CO_2–saturated conditions. The resultant phase diagrams can be used to predict the nature of mantle melting under conditions of saturation with different volatile species and hence over a range of f_{O_2}'s.

A pressure of 28 kbar was chosen to allow incorporation of the volatile–absent experimental data of WINDOM and BOETTCHER (1981) along the joins jadeite–enstatite (Jd–En) and jadeite–forsterite (Jd–Fo) as well as duplicating pressure conditions near the top of the oceanic LVZ where ≳2% partial melt is believed to exist (GREEN and LIEBERMANN, 1976). Experiments were conducted along the join $Ne_{55}Q_{45}$–$Ne_{55}Fo_{45}$ to provide approximately 90° intersection with the two–phase boundary at liquidus temperatures that are not prohibitively high (*i.e.*, <1500°C). Vapor saturation was confirmed in each experiment by piercing the sample capsule and noting the weight loss at 25°C and 110°C. All

water–saturated runs produced a fine white precipitate surrounding the fluid exit hole; this arises from solid-phase solubility in high pressure–temperature aqueous fluids as discussed by RYABCHIKOV *et al.* (1982).

Experimental charges were examined optically and by electron microprobe analysis; all showed quench effects of variable extent, mainly as $MgAl_2SiO_6$(MgTs)–rich pyroxene overgrowths sometimes extending to Jd–rich compositions and as individual crystallites on and about En_{ss}. Skeletal olivines are present in some runs. In selected experiments, electron microprobe analyses established liquid and crystal compositions as recorded in the Appendix and Table 2. In practice, only for the volatile–absent runs, showing the least quench effects and only small Na/Al ratio deviations from 1, were we able to analyse liquid compositions directly. This allowed the volatile–absent Fo–En_{ss} boundary to be well constrained with three experiments at $Ne_{55}Fo_{25}Q_{20}$. A liquid composition was estimated for CO_2–saturated run T–1227 from analysis of a large glass–rich area. The composition was projected back into the Na/Al = 1 plane from average quench En. In both H_2O-saturated and C–H fluid-saturated OH–containing glasses the combined effects of quench crystal growth and Na–volatilization under the electron microprobe beam precluded any estimate of liquid composition.

The position (in terms of weight percent Fo) of experimentally determined Fo–En_{ss} two–phase boundaries for the Ne_{55} compositions at P = 28 kbar are listed below:

Volatile species	Fo Weight percent	Estimated liquidus temperature (°C)
absent	24	1495 ± 5
H_2O–saturated	18 ± 1	1120 ± 15
CH_4–H_2–saturated	21 ± 1	1410 ± 15
CO_2–saturated	34 ± 1	1410 ± 15

These data allow delineation of Fo and En_{ss} liquidus phase fields on the ternary Ne–Fo–Q diagram (Figure 2); the volatile–absent fields for Jd_{ss}, Sp ($MgAl_2O_4$ spinel) and Ne_{ss} ($nepheline_{ss}$) are from GUPTA *et al.* (1987).

Volatile–absent boundary

The position of the volatile–absent two–phase boundary is consistent with the experimental results of KUSHIRO (1968) on the composition NFA–1 ($Ne_{62}Fo_{18}Q_{20}$) which has Fo on the liquidus up to 30 kbar. The intersection of the boundary with the Fo–Q binary system is estimated from the data of CHEN and PRESNALL (1975) to occur near Fo_{24}. These constraints place the Fo–En_{ss} boundary at 28 kbar close to the composition $Jd_{32}Fo_{68}$ on the Jd–Fo join. WINDOM and BOETTCHER (1981, Figure 2) inferred that this point should lie near $Jd_{50}Fo_{50}$ but this position could not be adequately constrained by their experimental data. Recent experimental work in the dry system by GUPTA *et al.* (1987) has refined the position of the three phase Fo–En_{ss}–Jd_{ss} point. Although differing from WINDOM and BOETTCHER's (1981) interpretation, it is in agreement with their experimental data along

Table 2. Sm and Jd composition glasses: experimental results at 30 kbar

Run #	Comp.	Volatile	T°C	Product
T–1158	Sm	absent	1420	Glass
T–1159	Sm	absent	1370	Sm crystals
T–1160	Sm	absent	1395	Glass
T–1178	Sm	CO_2 ~8 weight percent	1300	Clear glass (MH buffer)
T–1250	Sm	H_2O ~6 weight percent	1300	Clear glass (graphite capsule)
T–1318	Sm	C–H 9 weight percent	1320	Glass + grossular crystals
T–1341	Sm	C–H 9 weight percent	1350	Clear glass containing small fluid inclusions <1 μm diam.
T–1442	Sm/SiC	—	1500	Glass + disseminated graphite
T–1296	Jd	C–H 10 weight percent	1320	Clear glass, inclusion-free

Microprobe analyses:	SiO_2	Al_2O_3	CaO	Na_2O	Total
T–1341 (Av. glass)	44.2 (.4)*	18.6 (.4)	20.9 (.3)	11.8 (.2)	95.5
T–1296 (Av. glass)	56.0 (.6)	23.6 (.5)	—	14.7 (.2)	94.3
T–1318 (grossular)	39.48	22.56	37.56	0.00	99.6

* Figures in brackets are 1σ standard deviations.

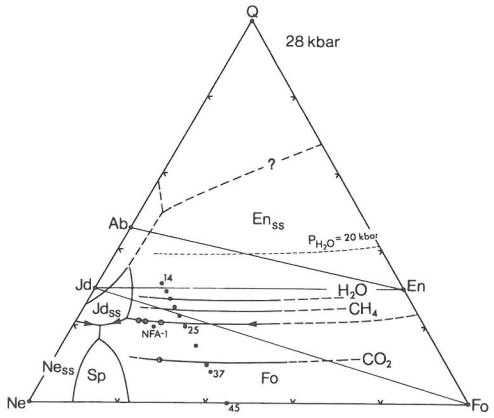

FIG. 2. Ternary liquidus phase diagram (weight percent) for the system Ne–Fo–Q at 28 kbar showing the position of the Fo–En_{ss} two-phase boundary under volatile-absent and CO_2, H_2O and CH_4–H_2 volatile-saturated conditions. Volatile-absent phase boundaries are from GUPTA *et al.* (1986) and this work. Dashed phase boundaries are inferred. Compositions studied are indicated by the filled circles on the join $Ne_{55}Fo_{45}$–$Ne_{55}Q_{45}$, adjacent numbers indicate weight percent Fo component. Composition NFA-1 is from KUSHIRO (1968) and the 20 kbar water-saturated Fo–En_{ss} boundary is from KUSHIRO (1972). Double circles are analysed liquid compositions.

the Jd–Fo and Jd–En joins as well as the earlier data of KUSHIRO (1968). Figure 3 presents the amended phase diagram for the Jd–Fo pseudobinary join. The main change from WINDOM and BOETTCHER (1981) is the expansion of the Fo + L phase field (note also that two points are mislabelled on their original figure).

CO_2-saturated boundary

The shift in position of the Fo–En_{ss} boundary relative to the volatile-absent system is greatest for CO_2-saturation (expansion of En_{ss} field from Fo_{24} to Fo_{34} at Ne_{55}) reflecting CO_2's strong melt polymerizing role. Equilibrium and quench En_{ss} compositions on this boundary are rich in MgTs component (equilibrium crystals contain 15–17 weight percent Al_2O_3) and poor in Na_2O (<3.5 weight percent). This behaviour may arise from a decrease in Na_2O activity in the melt due to sodium–carbonate complex formation and accords with the CO_2 solubility mechanisms discussed by MYSEN and VIRGO (1980b,c).

H_2O-saturated boundary

The depolymerizing role of H_2O dominated fluids is clearly illustrated in Figure 2. Expansion of the Fo phase field at Ne_{55} relative to the volatile-absent system is from $Fo_{24} \rightarrow Fo_{18}$. This shift is not as large as that for CO_2 in the opposite direction; however, there appears to be a substantial pressure effect associated with the H_2O-saturated boundary. At $P_{H_2O} = 20$ kbar this boundary is found near $Ne_{55}Fo_7Q_{38}$ (KUSHIRO, 1972) a difference of Fo_{11}

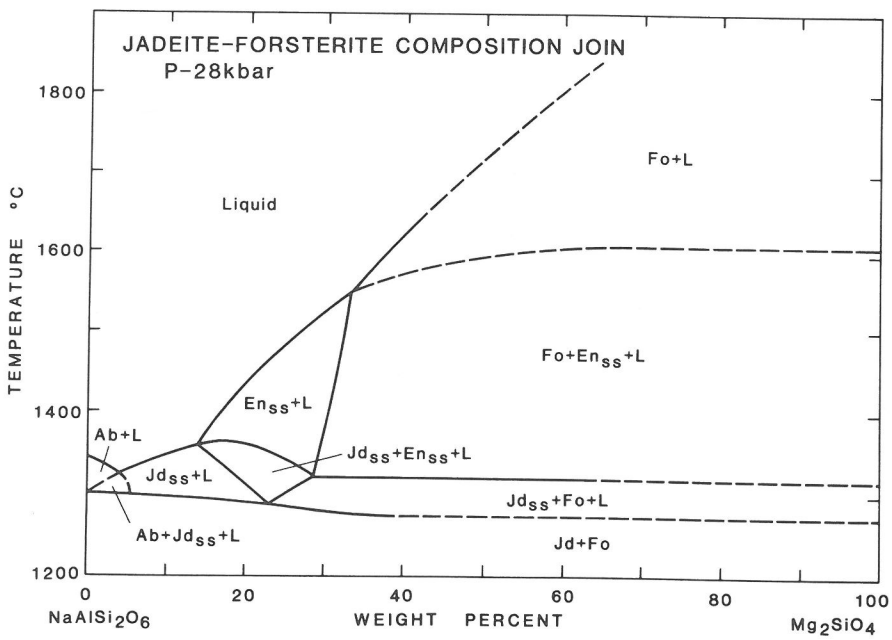

FIG. 3. Amended pseudobinary phase diagram for the join Jd–Fo at 28 kbar.

from the volatile-absent boundary at the same pressure (*cf.* the Fo_6 difference at 28 kbar). This effect may be ascribed to a diminishing ability of H_2O to depolymerize melts at higher pressures and could be due to a number of factors:

(a) changes in the solubility of solid components in co-existing aqueous fluid with pressure;

(b) dissolution of a higher proportion of H_2O in molecular form with increasing P_{H_2O} as shown by STOLPER (1982); because molecular water dissolves without (Si, Al)–O–Si bond cleavage there will be no accompanying network depolymerization;

(c) change in behaviour of H_2O with pressure toward that of a network polymerizer by formation of a greater proportion of alkali cation–hydroxy complexes relative to Si–OH bonds in an analogous fashion to CO_2 dissolution forming carbonate complexes.

If H_2O tends to be more polymerizing with increasing pressure via any of the above mechanisms, then there are important consequences for magma genesis. Thus, CO_2 may not be required in the genesis of highly silica undersaturated magmas (as proposed by EGGLER, 1978, and other workers) if H_2O can perform a melt polymerizing role. Further investigation of the role of H_2O at high pressures is clearly warranted.

C–H fluid—saturated boundary

The Fo–En_{ss} two-phase boundary for saturation with reduced C–H fluids falls between the H_2O and the volatile-absent boundaries implying a depolymerizing role for reduced C–H volatiles. The compositions of equilibrium, quench rim and quench crystal pyroxenes for volatile-absent, C–H fluid, H_2O and CO_2–saturated runs in which Fo and En_{ss} equilibrium crystals coexist are compared in Figures 4A and 4B. The proportion of jadeite component in equilibrium pyroxenes varies with volatile species in the order: CH_4–H_2 > volatile-absent > CO_2 > H_2O (circled in Figure 4B). This order is generally retained for quench rims and quench crystals. In the volatile-absent, CO_2 and C–H fluid—saturated cases, temperature and hence silica activity (buffered by coexisting Fo and En_{ss}), are of similar magnitude. On this basis, we would interpret differences in pyroxene chemistry as due largely to changes in the activity of network modifying oxides in the liquid. The observed enrichment in pyroxene of the jadeite component under conditions of C–H fluid saturation may, therefore, reflect an increase in the activity of network modifying Na_2O and Al_2O_3 relative to the volatile-absent system.

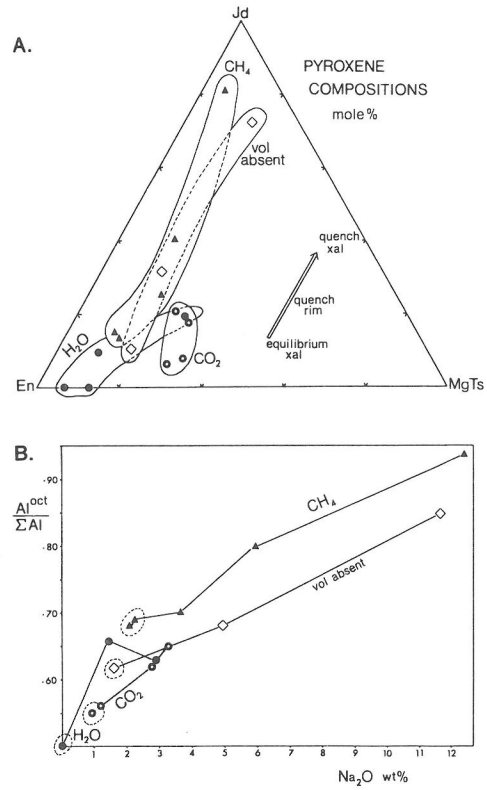

FIG. 4. A. Plot of pyroxene compositions (mol percent) coexisting with forsterite in selected runs in the system Ne–Fo–Q. Quench pyroxenes extend to very Jd-rich compositions in the CH_4 fluid—saturated and volatile-absent systems. ▲ C–H fluid—(*i.e.*, CH_4–H_2) saturated (T–1291); ◇ volatile-absent (T–1210); ◎ CO_2–saturated (T–1227); ● H_2O–saturated (T–1175). Arrow shows the direction of pyroxene quench trends. B. Plot of Al occupying octahedral sites/ΣAl versus Na_2O (weight percent) for pyroxenes of Figure 4A. Dotted areas indicate equilibrium pyroxenes.

The results presented here indicate that C–H volatile dissolution leads to network depolymerization accompanied by changes in the activity of network modifying oxides. In order to write a mechanism to describe the dissolution process, however, more detailed information on an atomic or molecular basis is needed than can be supplied by liquidus studies. This requires spectroscopic and analytical data on samples free from contamination as considered below.

SOLUBILITY MECHANISM OF METHANE: ANALYTICAL AND SPECTROSCOPIC CONSTRAINTS

Sodamelilite and jadeite compositions have been chosen for this investigation because their volatile–

free, H_2O and CO_2–containing glasses have been characterized structurally by x-ray diffraction and vibrational spectroscopic methods (*e.g.*, TAYLOR and BROWN, 1979; MYSEN and VIRGO, 1980a; MYSEN *et al.*, 1980; SHARMA and YODER, 1979). In addition, both compositions show good quenching behaviour in the presence of volatiles (MYSEN and VIRGO, 1980a).

Volatile–absent melting of sodamelilite and jadeite at 30 kbar

To determine the magnitude of liquidus depressions in the presence of C–H volatiles the volatile–free melting points of sodamelilite and jadeite are required at 30 kbar. Crystalline sodamelilite is stable above 4–5 kbar and at 10 kbar has a melting interval of ~50°C (YODER, 1964). At 20 kbar, the solidus and liquidus may be regarded as coincident within experimental precision (KUSHIRO, 1964). Experiments at 30 kbar (Table 2) show that crystalline sodamelilite melts congruently at 1380 ± 10°C. Jadeite melts congruently to liquid at 1370 ± 10°C, 30 kbar (BELL, 1964).

C–H saturated melting at 30 kbar

Results of the melting experiments at 30 kbar are listed in Table 2. Product glasses are clear and graphite-free. Interaction of C–H fluids and silicate melts leads to liquidus depressions of ~40°C in sodamelilite and at least 50°C in jadeite. This observation together with the consistently low electron microprobe totals reported in Table 2 implies a significant solubility of a reduced volatile component or components. All experimental charges retain excess carbide and mass spectra of quenched vapor indicate the presence of only trace quantities of bulk oxygen as H_2O. Thus the observed effects cannot be ascribed to absorbed H_2O or other external sources of oxidation.

In some experiments, small blebs of Pt–Si alloy were occasionally observed at the Pt capsule/silicate interface. This could be a potential source of oxygen (and hence H_2O) via the reaction:

$$x\mathrm{SiO_2(melt)} + y\mathrm{Pt(capsule)} \rightarrow \mathrm{Si}_x\mathrm{Pt}_y\mathrm{(alloy)} + x\mathrm{O_2}, \quad \text{where} \quad 0 < x, y < 1. \quad (2)$$

Electron microprobe analyses for silica (see Table 2), however, show no detectable Si loss to a Pt–Si alloy within analytical error: compare 46.5 weight percent SiO_2 in the sodamelilite starting material with 46.3 weight percent (std deviation 0.4) found in the C–H saturated glass (total normalized to 100%). The amount of oxygen (expressed in the form of dissolved H_2O) that could enter a sodamelilite melt by this process and remain undetected by silica analysis is <0.4 weight percent H_2O.

Under C–H fluid excess conditions the liquidus phase for the sodamelilite composition is grossular and not crystalline sodamelilite as observed under volatile–absent conditions. This observation is consistent with the early appearance of garnet on the liquidus of the C–H volatile—saturated $Di_{35}Py_{65}$ composition (EGGLER and BAKER, 1982). Combined with the results in the system Ne–Fo–Q these observations suggest that, in general, liquidus phases of higher octahedral aluminum content are favored by C–H fluid dissolution.

Spectroscopic results

Fourier Transform infrared (FTIR) spectra of sodamelilite and jadeite glasses are presented over

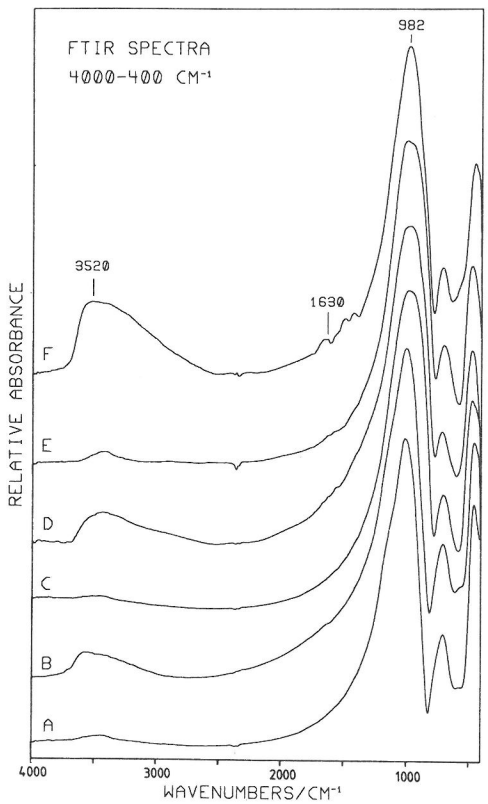

FIG. 5. FTIR spectra (4000–400 cm^{-1}): A. Volatile-free jadeite glass (quenched at 1 bar); B. C–H fluid—saturated jadeite glass (T–1296); C. Volatile-free sodamelilite glass (quenched at 30 kbar); D. C–H fluid—saturated sodamelilite glass (T–1341); E. Sodamelilite glass reduced by interaction with silicon carbide at 1500°C, 30 kbar (see text); F. Hydrous sodamelilite glass (T–1250). Weak positive or negative bands near 2350 cm^{-1} are due to atmospheric CO_2 vapour.

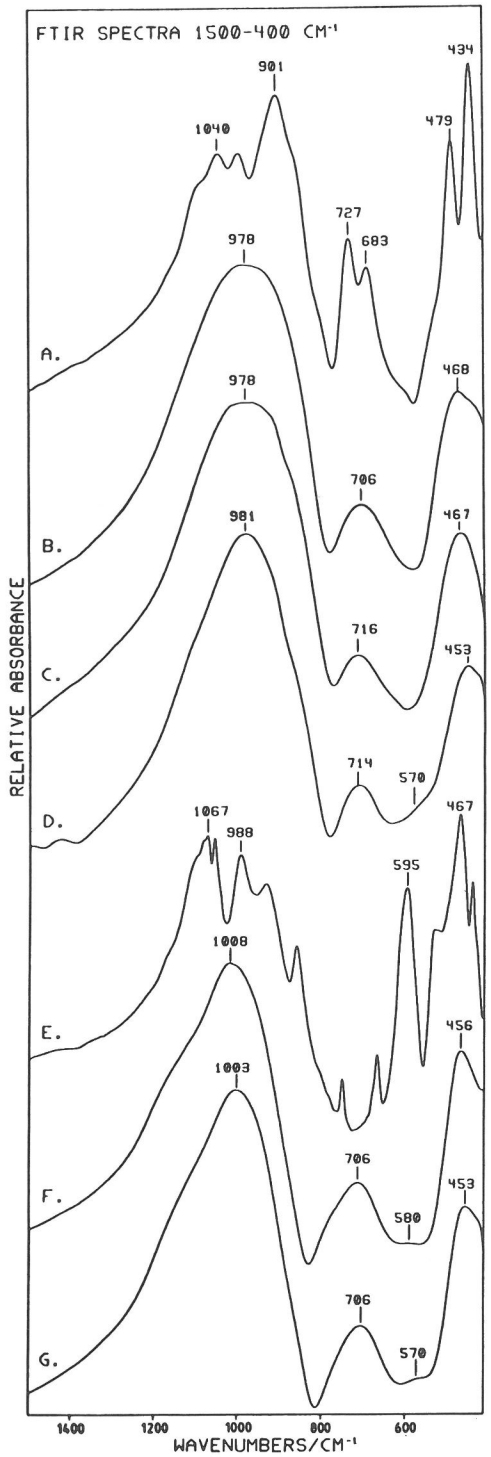

FIG. 6. FTIR spectra (1500–400 cm^{-1}): A. Crystalline sodamelilite (prepared at 30 kbar); B. Volatile-free sodamelilite glass (quenched at 30 kbar); C. C–H fluid—saturated sodamelilite glass (T–1341); D. Sodamelilite glass containing 5.5 ± 0.2 weight percent dissolved H_2O (T–1250). The doublet at 1500–1400 cm^{-1} is due to trace dissolved carbonate; E. Crystalline jadeite (prepared at 25 kbar); F. Volatile-free jadeite glass (quenched at 1 bar); G. C–H fluid—saturated jadeite glass (T–1296).

the ranges 4000–400 cm^{-1} and 1500–400 cm^{-1} in Figures 5 and 6. For jadeite, comparisons have been made between C–H fluid–saturated glass quenched from 30 kbar, 1320°C and the 1 bar volatile–absent jadeite glass. Such comparisons are valid because the Raman study of MYSEN *et al.* (1980) has shown that the spectroscopically resolvable structure of quenched jadeite melt remains essentially unaffected by pressure up to at least 38 kbar. For sodamelilite, the volatile–free glass used for comparison was quenched from 30 kbar, 1395°C. The following features distinguish spectra of the C–H fluid saturated glasses (Figs 5B, D and 6C, G) from the volatile–free glasses (Figures 5A, C and 6B, F):

High–frequency region 4000–1400 cm^{-1}

A broad, asymmetric O–H stretch band centered at ~3580 cm^{-1} is the most prominent feature in the high–frequency region. Comparison of O–H peak areas with hydrous sodamelilite glass (Figure 5F) containing 5.5 ± 0.2 weight percent H_2O gives an estimated dissolved hydrogen content equivalent to 2.7 ± 0.3 weight percent H_2O (if all H is derived from CH_4 then this would correspond to a methane solubility of ~1 weight percent). The area under the O–H envelope in C–H fluid—saturated jadeite suggests a similar dissolved OH content. There are no absorption bands at ~2900 cm^{-1} that could be ascribed to C–H bond stretching in dissolved molecular methane or other hydrocarbon groups such as $-CH_3$ or $-CH_2-$. No absorptions appear in the frequency range 2600–1700 cm^{-1}. A weak band appears at ~1630 cm^{-1} (ν_2 H–O–H bending vibration) due to the presence of dissolved molecular H_2O (STOLPER, 1982). There is no evidence for dissolved carbonate which has a characteristic ν_3 absorption band or bands at ~1600–1380 cm^{-1}.

Aluminosilicate envelopes 1200–400 cm^{-1}

Changes occur in both the high–frequency and mid-range envelopes (centered at ~1000 cm^{-1} and ~700 cm^{-1} respectively) and in the spectral region near 570 cm^{-1}. These changes reflect structural rearrangements in the aluminosilicate network that result from volatile dissolution. They are more clearly illustrated in difference spectra (volatile–saturated minus volatile–absent glasses) presented in Figure 7. Strong positive features appear at

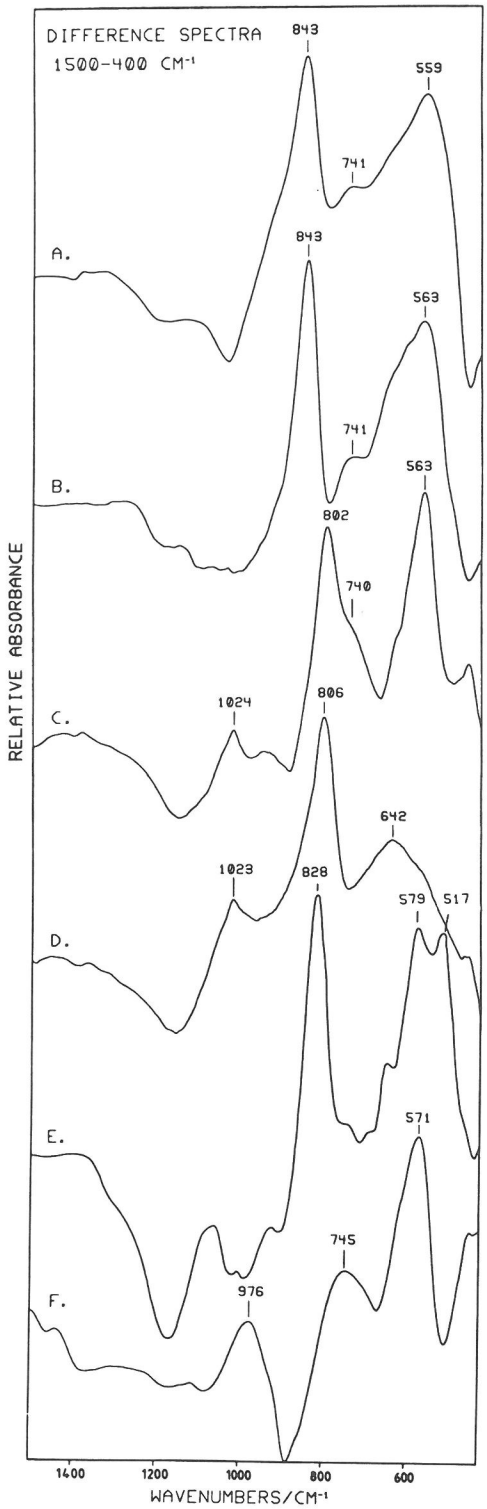

FIG. 7. Difference spectra (1500–400 cm^{-1}) (component-bearing) minus (component-absent): A. (C–H fluid—saturated jadeite glass T–1296) minus (1 bar volatile-free jadeite glass); B. Same as A but duplicate KBr discs were used to record both component-bearing and component-absent spectra (reproducibility check); C. (C–H fluid—saturated sodamelilite glass T–1341) minus (30 kbar volatile–free sodamelilite glass); D. (SiC reduced sodamelilite glass) minus (30 kbar volatile–free sodamelilite glass) [the "reduced component"]; E. (C–H fluid—saturated $Ne_{55}Fo_{25}Q_{20}$ glass containing ~10% enstatite crystals: run T–1289) minus ($Ne_{55}Fo_{25}Q_{20}$ 1 bar glass); F. (Hydrous sodamelilite glass T–1250) minus (30 kbar volatile–free sodamelilite glass) [the "oxidized component"].

~850–800 and ~570 cm^{-1} in C–H fluid—saturated sodamelilite and jadeite glasses. Weaker features are present as shoulders at ~950, ~740 and ~640 cm^{-1} and at ~1020 cm^{-1} in sodamelilite only. Both strong positive difference features appear in the spectrum of Ne–Fo–Q glass (sample from run T–1289) which also has a strong band at 517 cm^{-1} due the presence of crystalline enstatite. Negative difference features are much less pronounced and occur in spectra of both C–H fluid–saturated sodamelilite and jadeite at ~1160 cm^{-1} and in jadeite near 1050 cm^{-1}. These may be due to a decrease of Si–O–(Si, Al) bridging bonds but it is difficult to make specific assignments because of the complex overlapping nature of Si–O symmetric and asymmetric stretching modes of both bridging and non-bridging oxygen in this region of the infrared spectrum. There is little change in the low-frequency envelopes (centred near 450 cm^{-1}) except at <425 cm^{-1} where KBr background effects become noticeable.

Positive difference features related to OH dissolution

The prominent 570 cm^{-1} band is present in the FTIR difference spectrum of hydrous sodamelilite glass (Figure 7F) and therefore may be ascribed to changes in the aluminosilicate network resulting from OH dissolution. Bands in this region in the Raman spectra of aluminosilicate glasses have usually been assigned to in–plane Si–O–Si bridge bending motions or to the presence of 3– or 4–membered ring structures (MCMILLAN, 1984). However, in the 500–600 cm^{-1} region in the infrared TARTE (1965, 1967), FARMER *et al.* (1979) and SERNA *et al.* (1979) have assigned strong absorption bands in aluminosilicate glasses, crystals and gels to vibrations of AlO_6 polyhedra. While such an assignment will require confirmation (perhaps using more definitive techniques such as solid–state NMR), TAYLOR (1985) noted that strong IR bands in the 620–520 cm^{-1} region are found in all crystalline aluminosilicates containing AlO_6 polyhedra

but are absent in structurally related minerals lacking Al or in those containing only AlO_4 polyhedra (exceptions are minerals based on small ring framework structures such as the feldspars or scapolites). This is illustrated (Figures 6A & 6E) in the spectra of crystalline jadeite ($NaAl^{VI}Si_2O_6$, strong band at 595 cm^{-1}) and sodamelilite ($NaCaAl^{IV}Si_2O_7$, no strong absorptions 620–520 cm^{-1}). The weaker 950 and 740 cm^{-1} features identified in the C–H fluid —saturated glasses are also present in the hydrous glass and could be due, respectively, to Si–OH stretching (MYSEN and VIRGO, 1980a) and vibrations of Al–O–Al linkages in aluminate condensates or "clusters" (TARTE, 1967; SERNA *et al.*, 1977).

850–800 cm^{-1} positive difference feature

The ~850–800 cm^{-1} feature is located on the low-frequency limb of the high-frequency envelope in jadeite, sodamelilite and Ne–Fe–Q glasses. This band is not present in hydrous sodamelilite glass and therefore is unlikely to be associated with OH dissolution or network depolymerization. Instead, this band is characteristic of reduced C–H volatile dissolution and may be due to a dissolved reduced component. Spectroscopic identification of such a component in aluminosilicate glasses is verifiable experimentally as discussed later. Possible assignments for the 850–800 cm^{-1} feature are considered below after applying necessary theoretical constraints.

Theoretical constraints

Mechanisms for the dissolution of reduced volatiles in silicate melts have been suggested by very few authors. In a study that investigated the solubility behaviour of CO as a CO_2–CO volatile mixture, EGGLER *et al.* (1979) suggested that CO dissolves by a carbonation reaction of the type:

$$CO + 2O^- = CO_3^{2-} \quad \cdots\cdot A, \quad (3)$$

where "O^-" = non-bridging oxygen. EGGLER and BAKER (1982) proposed two mechanisms for CH_4 dissolution based on analogous reactions for H_2O, *i.e.*

$$4Si\text{–}O\text{–}Si + CH_4 = 4Si\text{–}OH + C \quad \cdots\cdot B \quad (4)$$

$$Si\text{–}O\text{–}Si + CH_4 = Si\text{–}CH_3 + Si\text{–}OH \quad \cdots\cdot C. \quad (5)$$

The validity of mechanisms A and B is, however, questionable because neither reaction can be correctly charge-balanced (at least in a chemically realistic sense in Equation A, "O^-" cannot be equated with NBO for usual oxidation states of oxygen in silicate melts). Because electroneutrality should always be obeyed when balancing any chemical reaction, it is evident that if a reduced volatile dissolves in a silicate melt to give an "oxidized bond" such as O–H or O–C, then this must be balanced at equilibrium by concurrent production of a "reduced bond." Such a bond is one involving an element in a lower oxidation state or one excluding oxygen or both. Candidates in the case of a C–H fluid could include: Si–H, Si–C, C–H, Si–Si and analogous bonds involving Al and other metal cations.

Reference to the FTIR spectra of sodamelilite and jadeite C–H fluid–saturated glasses immediately eliminates metal–hydrogen or C–H bonds as candidates for the "reduced bond." This is because bonds of this type have characteristic IR stretching frequencies in the range ~3000–1700 cm^{-1} where no absorption was noted. C–H bonds are expected at 3050–2850 cm^{-1} and Si–H bonds at 2250–2100 cm^{-1} (POUCHERT, 1981). Thus reaction C, suggested by EGGLER and BAKER (1982), while being properly charge balanced and involving Si–C and C–H as reduced bonds, is not consistent with observed spectroscopic results.

Possible mechanisms of C–H volatile dissolution

The theoretical and spectroscopic constraints discussed above, greatly limit the choice of a reduced component. We suggest that the most likely candidates are either (I) a network unit containing Si–C bonds or (II) a non-stoichiometric network component containing units having an O/Si ratio less than 2, such as found in amorphous silicon monoxide. The former alternative implies that only hydrocarbon species (*i.e.*, dominantly CH_4) are involved in the dissolution process, whereas the latter alternative is a general reduction of the silicate network and could involve H_2 as well as CH_4. Support for candidate (I) is given by the known range of IR active Si–C bond stretching frequencies for molecular compounds (WELTNER and MCLEOD, 1964; POUCHERT, 1981) *e.g.*, organosilicon compounds (Si–CH_3 bonds): 680–740 cm^{-1}; matrix-isolated SiC_2 and SiC molecules: 835 and 1226 cm^{-1} respectively. The range ~700 cm^{-1} to 1226 cm^{-1} encompasses the region that includes the strongest difference spectrum features at ~850–800 cm^{-1}. However, these features would also be consistent with the presence of silicon monoxide or related units. Compared with pure silica glass, the high-frequency envelope in amorphous silicon monoxide is shifted down frequency by some 100 cm^{-1} (PLISKIN and LEHMAN, 1965; KHANNA *et al.*, 1981). A similar shift in band components in aluminosilicate

glasses would be sufficient to extend the high-frequency envelope to lower wavenumbers and hence result in the observed ~850–800 cm^{-1} positive difference features.

Mechanisms (I) and (II) may be described by the following balanced equations (for $[SiO_3]^{2-}$ and sodamelilite melt-units):

Mechanism I: (Silicon–carbon bond formation)

$$\left.\begin{aligned} &2[SiO_3]^{2-} + CH_4 \\ &\quad = \{Si\text{–}C\} + 4[OH]^- + [SiO_2]^0 \quad (6) \\ &2[Al^{IV}Si_2O_7]^{3-} + CH_4 = 2[Al^{NN}O_2]^- \\ &\quad + 4[OH]^- + \{Si\text{–}C\} + 3[SiO_2]^0 \quad (7) \end{aligned}\right] \cdots\cdot D.$$

Mechanism II: (Network reduction by CH_4 or H_2, or both)

$$\left.\begin{aligned} &2[SiO_3]^{2-} + CH_4 \\ &\quad = 2\{Si\text{–}O\} + 4[OH]^- + \{C^0\} \quad (8) \\ &2[Al^{IV}Si_2O_7]^{3-} + CH_4 \\ &\quad = 2[Al^{NN}O_2]^- + 4[OH]^- \\ &\quad + 2\{Si\text{–}O\} + 2[SiO_2]^0 + \{C^0\} \quad (9) \end{aligned}\right] \cdots\cdot E$$

$$\left.\begin{aligned} &[SiO_3]^{2-} + H_2 = \{Si\text{–}O\} + 2[OH]^- \quad (10) \\ &[Al^{IV}Si_2O_7]^{3-} + H_2 = [Al^{NN}O_2]^- \\ &\quad + 2[OH]^- + \{Si\text{–}O\} + [SiO_2]^0 \quad (11) \end{aligned}\right] \cdots\cdot F$$

where

{ } = unidentified location in silicate network
[ ] = melt-unit or complex
$\{C^0\}$ = graphite, diamond or carbon dissolved in the melt in unspecified form
NN = Al in non-network sites (*e.g.*, AlO_6 polyhedra).

For both mechanisms additional equilibria can be written to relate spectroscopically observed species such as dissolved molecular water:

$$[SiO_2] + 2[OH]^- = [H_2O]_{molecular} + [SiO_3]^{2-}. \quad (12)$$

Mechanisms (I) and (II) are similarly constructed; both reactions produce 4 moles of O–H bonds (the "oxidized component") per mole of dissolved methane. For the sodamelilite melt-unit, the solution process is written to accommodate a redistribution of Al between network and non-network sites. The major difference between the mechanisms is in the nature of the reduced bond formed (*i.e.*, the "reduced component"). In mechanism (I), a significant melt-phase solubility of reduced carbon as Si–C bonds is implied. This mechanism is directly analogous to the structural role of nitrogen in Na_2O–CaO–silicon oxynitride glasses recently investigated by BROW and PANTANO (1984). Based on FTIR and x-ray photoelectron spectroscopic results those authors concluded that nitrogen is present in the silicate network of oxynitride glasses in the form of Si–N bonds with N in three-fold and possibly two-fold co-ordination sites. With increasing N content the principle changes in the FTIR spectra are seen in the high-frequency envelope which broadens and shifts to lower wavenumbers (similar to that observed in the C–H fluid—saturated glasses). The maximum amount of nitrogen dissolved in the Na_2O–CaO–silicon oxynitride glasses at 1 bar was ~2.2 weight percent N but the effects of N substitution on the network are clearly seen in the FTIR spectrum at much lower levels.

Mechanism (II) requires the presence of a silicate network unit with an O:Si ratio <2; this is represented in Equations E and F by a {SiO} or "silicon monoxide" group. It is conceivable that such units might resemble those found in amorphous silicon monoxide. The RDF study of YASAITIS and KAPLOW (1972) favors a structure for this compound based on puckered $(SiO)_n$ rings where the average co-ordination number about each Si atom does not deviate significantly from two. Such a structure gives each Si atom a formal valency of II.

Characterization of the "reduced component"

For the sodamelilite composition the "reduced component" was characterized spectroscopically by reducing the silicate network at high pressure under anhydrous conditions. The starting material consisted of sodamelilite glass in which a portion of the SiO_2 was substituted by –SiC [total C = 1.5 weight percent, equivalent to a methane solubility of 2 weight percent via mechanism (I)]. An inner graphite capsule was used to separate the silicate/carbide mix from the outer Pt capsule to prevent Pt–Si alloy formation. Over a run time of 90 min at 30 kbar and 1500°C, SiC was fully decomposed producing a product consisting of clear glass and disseminated graphite. This experiment does not distinguish between mechanisms (I) and (II) because SiC may dissolve to form reduced Si–C bonds or may reduce the silicate network directly via the reaction: $SiC + SiO_2 \rightarrow 2\{SiO\} + C$ [analogous to mechanism (II)]. FTIR spectra are shown in Figures 5E and 7D. Graphite is essentially IR inactive over this spectral range and does not contribute to the observed bands. The difference spectrum Figure 7D has a major positive feature at 806 cm^{-1} and weaker features at 1023 and 642 cm^{-1} corresponding closely

to those present in C–H fluid—saturated sodamelilite. In fact a combination of the hydrous sodamelilite glass difference spectrum (the "oxidized component") and Figure 7D would be almost indistinguishable from the C–H fluid—saturated spectrum. Thus separate "reduced" and "oxidized" components can be characterized spectroscopically; the latter is associated with O–H bond formation and the former is best interpreted as a reduction of the silicate network. Whether or not this reduction involves formation of reduced bonds to carbon must be decided by analytical means.

Analytical constraints

Results of pyrolysis/gas chromatography analyses for C and H for both samples and standards are presented in Table 1. The analysed carbon contents of the standards (SiO_2–SiC mixtures) are between half and one third of the known amounts present. This suggests incomplete oxidation of SiC has occurred with greatest discrepancy occurring at C contents >0.5 weight percent. Carbon values for the glass unknowns must therefore be regarded as minimum quantities only; if α–SiC forms metastably in these samples then analyses may be low by as much as a factor of two for total C contents ≤0.5 weight percent. Hydrogen analyses (converted to weight percent H_2O) are in good agreement with those deduced spectroscopically for sodamelilite. C–H fluid equilibrated glasses therefore contain a minimum of ~1000 ppm C and a maximum of ~2000 ppm C. These results are confirmed by quantitative and semi-quantitative electron microprobe analyses for carbon (Table 3). Carbon contents in the C–H fluid—saturated glasses are near or below the limit of detection (<2000 ppm) consistent with the gas chromatographic analyses.

For mechanism (I) to operate a reduced carbon solubility of 8000–12000 ppm is required. Thus mechanism (II) is supported as the dominant process for reduced volatile interaction with aluminosilicate melts. The small amount of carbon detected could dissolve either by mechanism (I) or perhaps in the form of atomic carbon occupying interstitial sites or cation vacancies as suggested FREUND *et al.* (1980) for oxide and silicate lattices. Carbon dissolved in this manner would be undetectable by IR and Raman spectroscopic methods.

Table 3. Microprobe analyses for carbon*

Sample	Expected weight percent	Weight percent analysed
Graphite (treated as unknown)	100.00	101.22
T-1178 (Sm + CO_2)	2.1 ± 0.2	2.15
T-1296 (Jd + C–H fl.)		
T-1341 (Sm + C–H fl.)	~0.1–0.2	≤0.2†
T-1318 (Sm + C–H fl.)		

* B.J. Griffin, analyst.
† Limit of detection ≃0.2 weight percent.

DISCUSSION

The recognition of mechanism (II) as the dominant process of C–H volatile solubility does not discriminate between the particular reduced volatile species involved. The mechanism is a general reduction of the silicate network that may take place in the presence of any of the reduced volatiles H_2, CH_4 or C_2H_6. In the presence of CH_4–rich fluids the H/C ratio of the melt phase greatly exceeds H/C of the coexisting fluid suggesting that reduced C–H volatile solubility will largely be a function of f_{H_2} and governed by equilibria similar to F above [Equations (10) and (11)]. In the system aluminosilicate–C–O, carbon monoxide is an important reduced volatile at $P < 20$ kbar and is believed to dissolve in melts by a carbonation reaction (EGGLER *et al.*, 1979). Charge balance constraints dictate a solubility mechanism that must involve a reduced component and we can propose reactions analogous to Equations E and F to describe CO dissolution, *e.g.*,

$$CO + [SiO_3]^{2-} = CO_3^{2-} + \{Si\text{–}O\}. \qquad (12)$$

If carbonate ions and a reduced melt component such as $\{SiO\}$ cannot coexist stably in silicate melts, there are real difficulties in proposing CO as a melt-soluble species other than in molecular form. Choice of mechanism (II) also helps rationalize the experimental results of LUTH and BOETTCHER (1986) which show that H_2 gives rise to significant depressions of the albite and diopside solidii implying a strong interaction between H_2 and aluminosilicate liquids as predicted by model F above.

Liquidus phase relations in the system Ne–Fo–Q suggest that dissolution of a C–H fluid, compared to the volatile-absent case, raises melt activities of network modifying Al_2O_3. This is in accord with the observed expansion of the garnet phase volume in other systems. The idea that carbon-rich eclogites could be the products of fractional crystallization of mantle melts under conditions of CH_4–H_2O–H_2 volatile saturation as proposed by EGGLER and BAKER (1982) is supported by the data presented here. KUSHIRO and YODER (1974) stated that ". . . in the presence of water . . . it should be possible for eclogite to form from garnet lherzolite" at depths

greater than the 26 kbar limit in the volatile-absent case, *i.e.*, to within the stability field of diamond. Because both H_2O and CH_4–H_2 fluids have similar melt depolymerizing behaviour, the findings of KUSHIRO and YODER (1974) will apply equally well to CH_4–H_2O–H_2 volatile mixtures as to pure H_2O. The added advantage in the case of carbon-rich eclogites is that the preference of the melt for H compared with C will drive a coexisting CH_4-bearing fluid phase toward carbon saturation leading to precipitation of diamond or graphite via equations similar to E. This is in accord with the origins of graphite-diamond eclogite from the Roberts Victor kimberlite as discussed by HATTON and GURNEY (1979). Those authors propose an origin based on rapid crystallization of melts produced by volatile-induced partial melting of garnet lherzolite where melt volumes are such that gravitational separation of diamond or graphite is ineffective. Whereas the authors propose that carbon is a result of reduction of a CO_2-bearing vapor during cooling, an alternative mechanism in which CH_4–H_2O–H_2 fluids give rise to melting accompanied by carbon precipitation from the fluid phase can equally well explain the origin of these rocks.

The finding that the network portion of silicate melts is quite susceptible to reduction via formation of groups with O/Si < 2, has not been demonstrated previously. For the observed H_2O content of C–H fluid-saturated sodamelilite glass at 30 kbar, 1350°C, we calculate that ~20% of the Si should be present as Si(II) (equivalent to 6–7 weight percent SiO) by mechanism (II). Reduced systems such as the enstatite chondrite group of meteorites have intrinsic oxygen fugacities that lie below IW. Measured values for the equilibrated EL enstatite chondrite group give f_{O_2}'s in the range ~IW–3 to IW–4 log f_{O_2} units (BRETT and SATO, 1984; WALTER and DOAN, 1969), near the redox conditions of the present C–H fluid experiments. In these rocks Si is distributed amongst three phases: metal (kamacite with ~1–4 weight percent Si), silicate (mainly enstatite), and silicon oxynitride (sinoite, $Si_2N_2O_2$) with graphite and not silicon carbide as an important accessory (SEARS *et al.*, 1982). This solid phase distribution of Si redox environments (at least at relatively low pressures) is consistent with the interpretation of C–H fluid—equilibrated aluminosilicate glasses where a reduced silicate network plus elemental carbon is evidently more stable than the equivalent melt structure containing Si–C bonds. It is possible to express the relationship between solid phases and a corresponding melt at $f_{O_2} \sim$ IW–4 × log f_{O_2} units via a disproportionation equilibrium of the type:

$$2[Si^{2+}O_x]_{\substack{\text{silicate}\\\text{melt}}} = (2-x)[Si^0]_{\substack{\text{metallic}\\\text{phase}}} + x[Si^{4+}O_2]_{\substack{\text{solid}\\\text{silicate}}} \quad (13)$$

where $1 < x < 2$.

In view of recent hypotheses supporting the early incorporation of large amounts of reduced enstatite chondritic components into the Earth's mantle (SMITH, 1982; JAVOY and PINEAU, 1983; ITO *et al.*, 1984) such equilibria are expected to have an important bearing on the mantle–core segregation of Si.

SUMMARY

In this investigation, a mechanism for C–H volatile solubility in aluminosilicate melts has been proposed from the interpretation of FTIR spectra within theoretical and analytical constraints. The mechanism is supported by phase relations determined in the system Ne–Fo–Q–C–O–H which indicates a melt depolymerizing role for C–H fluids.

On spectroscopic and theoretical grounds reduced C–H volatile dissolution can be resolved into soluble oxidized and reduced components. The former is represented by O–H bonds (as hydroxyl groups and molecular water) and affects melt structure much in the manner of H_2O dissolution. There is no spectroscopic evidence for the presence of dissolved molecular CH_4 or carbonate. The reduced component is somewhat enigmatic. Analytical data establish that the reduced component is consistent with a network silicon-oxygen unit where the formal valency on silicon is reduced from IV to II (O:Si stoichiometry of the system <2). At the f_{O_2} conditions of these experiments, ~IW–4.5 log f_{O_2} units, a general reduction of the silicate network is evidently favored over formation of Si–C bonds. This is not the case, however, in analogous reduced systems containing nitrogen where Si–N bonding in silicon oxynitride glasses is well characterized. Nevertheless, the reduced carbon solubility in the aluminosilicate melts studied is ~1000 ppm (minimum) in a form yet to be characterized.

These results have been used to (1) propose solubility mechanisms for other reduced volatiles such as CO; (2) help rationalize the observed strong interaction between H_2 and silicate melts; (3) suggest an alternative interpretation for the origin of carbonaceous eclogites as the product of CH_4–H_2O fluid-induced partial melts of garnet lherzolite; (4) suggest a mechanism for mantle–core partitioning of Si and (5) provide a basis for investigating the nature of melting in a reduced mantle as discussed in the accompanying paper by GREEN *et al.* (1987).

Acknowledgements—We are grateful to Dr. B. J. Griffin (University of Adelaide) for much time spent at the microprobe analysing our samples for carbon. We thank J. Bignell, N. Davis, W. Jablonski and K. L. Harris for invaluable technical assistance. This study was supported financially by a Commonwealth Postgraduate Scholarship and Australian National Research Fellowship awarded to WRT and an ARGS grant to DHG.

REFERENCES

ANDERSON A. T. (1975) Some basaltic and andesitic gases. *Rev. Geophys. Space Phys.* **13,** 37–55.

ARCULUS R. J. and DELANO J. W. (1981) Intrinsic oxygen fugacity measurements: techniques and results for spinels from upper mantle peridotites and megacryst assemblages. *Geochim. Cosmochim. Acta* **45,** 899–913.

BELL P. M. (1964) High-pressure melting relations for jadeite composition. *Carnegie Inst. Wash. Yearb.* **63,** 171–174.

BRETT R. and SATO M. (1984) Intrinsic oxygen fugacity measurements on seven chondrites, a pallasite, and a tektite and the redox state of meteorite parent bodies. *Geochim. Cosmochim. Acta* **48,** 111–120.

BREY G. (1976) CO_2 solubility and solubility mechanisms in silicate melts at high pressures. *Contrib. Mineral. Petrol.* **57,** 215–221.

BROW R. K. and PANTANO C. G. (1984) Nitrogen coordination in oxynitride glasses. *J. Amer. Ceram. Soc. Comm.* **67,** C72–C74.

CHEN C-H. and PRESNALL D. C. (1975) The system Mg_2SiO_4–SiO_2 at pressures up to 25 kilobars. *Amer. Mineral.* **60,** 398–406.

EGGLER D. H. (1978) The effect of CO_2 upon partial melting of peridotite in the system Na_2O–CaO–Al_2O_3–MgO–SiO_2–CO_2 to 35 kb, with an analysis of melting in a peridotite–H_2O–CO_2 system. *Amer. J. Sci.* **278,** 305–343.

EGGLER D. H. and BAKER D. R. (1982) Reduced volatiles in the system C–O–H: Implications to mantle melting, fluid formation and diamond genesis. In *High Pressure Research in Geophysics,* (eds. S. AKIMOTO and M. H. MANGHANI), pp. 237–250 Center for Academic Publications.

EGGLER D. H., MYSEN B. O., HOERING T. C. and HOLLOWAY J. R. (1979) The solubility of carbon monoxide in silicate melts at high pressures and its effect on silicate phase relations. *Earth Planet. Sci. Lett.* **43,** 321–330.

FARMER V. C., FRASER A. R. and TAIT J. M. (1979) Characterisation of the chemical structures of natural and synthetic aluminosilicate gels and sols by infrared spectroscopy. *Geochim. Cosmochim. Acta* **43,** 1417–1420.

FREUND F., KATHREIN H., WENGELER H., KNOBEL R. and HEINEN H. J. (1980) Carbon in solid solution in forsterite—a key to the intractable nature of reduced carbon in terrestrial and cosmogenic rocks. *Geochim. Cosmochim. Acta* **44,** 1319–1333.

GREEN D. H. and LIEBERMANN R. C. (1976) Phase equilibria and elastic properties of the pyrolite model for the oceanic upper mantle. *Tectonophys.* **32,** 61–92.

GREEN D. H. and RINGWOOD A. E. (1967) The genesis of basaltic magmas. *Contrib. Mineral. Petrol.* **15,** 103–190.

GREEN D. H., FALLOON T. J. and TAYLOR W. R. (1987) Mantle derived magmas—roles of variable source peridotite and variable C–H–O fluid compositions. In *Magmatic Processes: Physicochemical Principles,* (ed. B. O. MYSEN), The Geochemical Society Spec. Publ. No. 1, pp. 139–154.

GUPTA A. K., TAYLOR W. R. and GREEN D. H. (1987) Experimental study of the system forsterite–nepheline–jadeite at variable temperatures under 28 kbar pressure. *Amer. J. Sci.,* (Submitted).

HATTON C. J. and GURNEY J. J. (1979) A diamond-graphite eclogite from the Roberts Victor Mine. *Proc. Int. Kimberlite Conf., 2nd,* Vol. 2, 29–36.

HOLLOWAY J. R. (1981) Volatile interactions in magmas. *Adv. Phys. Geochem.* **1** (ed. S. K. SAXENA), pp. 273–293. Springer-Verlag.

HOLLOWAY J. R. and REESE R. L. (1974) The generation of N_2–CO_2–H_2O fluids for use in hydrothermal experimentation. I. Experimental method and equilibrium calculations in the C–O–H–N system. *Amer. Mineral.* **59,** 587–597.

ITO E., TAKAHASHI E. and MATSUI Y. (1984) The mineralogy and chemistry of the lower mantle: an implication of the ultrahigh-pressure phase relations in the system MgO–FeO–SiO_2. *Earth Planet. Sci. Lett.* **67,** 238–248.

JAKOBSSON S. (1984) Melting experiments on basalts in equilibrium with a graphite-iron-wustite buffered C–O–H fluid. Ph.D. Dissertation, Arizona State Univ.

JAVOY M. and PINEAU F. (1983) Stable isotope constraints on a model Earth from a study of mantle nitrogen. *Meteoritics* **18,** 320.

KHANNA R. K., STRANZ D. D. and DONN B. (1981) A spectroscopic study of intermediates in the condensation of refractory smokes: Matrix isolation experiments of SiO. *J. Chem. Phys.* **74,** 2108–2115.

KUSHIRO I. (1964) The join akermanite-soda melilite at 20 kilobars. *Carnegie Inst. Wash. Yearb.* **63,** 90–92.

KUSHIRO I. (1968) Compositions of magmas formed by partial zone melting of the Earth's upper mantle. *J. Geophys. Res.* **73,** 619–634.

KUSHIRO I. (1972) Effect of water on the composition of magmas formed at high pressures. *J. Petrol.* **13,** 311–334.

KUSHIRO I. and YODER H. S. JR. (1974) Formation of eclogite from garnet lherzolite: liquidus relations in a portion of the system $MgSiO_3$–$CaSiO_3$–Al_2O_3 at high pressures. *Carnegie Inst. Wash. Yearb.* **73,** 266–269.

LUTH R. W. and BOETTCHER A. L. (1986) Hydrogen and the melting of silicates. *Amer. Mineral.* **71,** 264–276.

MATHEZ E. A. and DELANEY J. R. (1981) The nature and distribution of carbon in submarine basalts and peridotite nodules. *Earth Planet. Sci. Lett.* **56,** 217–232.

MCMILLAN P. (1984) Structural studies of silicate glasses and melts—applications and limitations of Raman spectroscopy. *Amer. Mineral.* **69,** 622–644.

MCMILLAN P. (1985) Vibrational spectroscopy in the mineral sciences. In *Reviews in Mineralogy, 14* (eds. A. NAVROTSKY and S. KIEFFER), pp. 9–63 Mineralogical Society of America.

MYSEN B. O. and VIRGO D. (1980a) Solubility mechanism of water in basalt melt at high pressures and temperatures: $NaCaAlSi_2O_7$–H_2O as a model. *Amer. Mineral.* **65,** 1176–1184.

MYSEN B. O. and VIRGO D. (1980b) The solubility behaviour of CO_2 in melts on the join $NaAlSi_3O_8$–$CaAl_2Si_2O_8$–CO_2 at high pressures and temperatures: A Raman spectroscopic study. *Amer. Mineral.* **65,** 1166–1175.

MYSEN B. O. and VIRGO D. (1980c) Solubility mecha-

nisms of carbon dioxide in silicate melts: A Raman spectroscopic study. *Amer. Mineral.* **65,** 885–899.

MYSEN B. O., VIRGO D. and SCARFE C. M. (1980) Relations between anionic structure and viscosity of silicate melts—a Raman spectroscopic study. *Amer. Mineral.* **65,** 690–710.

PLISKIN W. A. and LEHMAN H. S. (1965) Structural evaluation of silicon oxide films. *J. Electrochem. Soc.* **112,** 1013–1019.

POUCHERT C. J. (1981) *The Aldrich Library of Infrared Spectra.* 3rd ed., 1203 pp. Aldrich Chemical Co.

ROCHOW E. G. (1973) The chemistry of silicon. In *Comprehensive Inorganic Chemistry,* Vol. 9, pp. 1323–1467 Pergamon Press.

RYABCHIKOV I. D., GREEN D. H., WALL V. J. and BREY G. P. (1981) The oxidation state of carbon in the reduced–velocity zone. *Geochem. Int.* **18,** 148–158.

RYABCHIKOV I. D., SCHREYER W. and ABRAHAM K. (1982) Compositions of aqueous fluids in equilibrium with pyroxenes and olivines at mantle pressures and temperatures. *Contrib. Mineral. Petrol.* **79,** 80–84.

RYERSON F. J. (1985) Oxide solution mechanisms in silicate melts: Systematic variations in the activity coefficient of SiO_2. *Geochim. Cosmochim. Acta* **49,** 637–650.

SEARS D. W., KALLEMEYN G. W. and WASSON J. T. (1982) The compositional classification of chondrites: II. The enstatite chondrite group. *Geochim. Cosmochim. Acta* **46,** 597–608.

SERNA C. J., VELDE B. D. and WHITE J. L. (1977) Infrared evidence of order–disorder in amesites. *Amer. Mineral.* **62,** 296–303.

SERNA C. J., WHITE J. L. and VELDE B. D. (1979) The effect of aluminium on the infra-red spectra of 7 Å trioctahedral minerals. *Mineral. Mag.* **43,** 141–148.

SHARMA S. K. and YODER H. S. JR. (1979) Structural study of glasses of akermanite, diopside and sodium melilite compositions by Raman spectroscopy. *Carnegie Inst. Wash. Yearb.* **78,** 526–532.

SMITH J. V. (1982) Heterogeneous growth of meteorites and planets, especially the Earth and moon. *J. Geol.* **90,** 1–125.

STOLPER E. (1982) Water in silicate glasses: an infrared spectroscopic study. *Contrib. Mineral. Petrol.* **81,** 1–17.

TARTE P. (1965) The determination of cation co-ordination in glasses by infra-red spectroscopy. In *Physics of Non-Crystalline Solids,* (ed. J. A. PRINZ), pp. 549–565. John Wiley.

TARTE P. (1967) Infra-red spectra of inorganic aluminates and characteristic vibrational frequencies of AlO_4 tetrahedra and AlO_6 octahedra. *Spectrochim. Acta* **23A,** 2127–2143.

TAYLOR M. and BROWN G. E. (1979) Structure of mineral glasses—II. The SiO_2–$NaAlSiO_4$ join. *Geochim. Cosmochim. Acta* **43,** 1467–1473.

TAYLOR W. R. (1985) The role of C–O–H fluids in upper mantle processes: a theoretical, experimental and spectroscopic study. Ph.D. Thesis, Univ. of Tasmania.

TAYLOR W. R. (1987) A 5-parameter modified Redlich-Kwong equation of state for C–O–H fluids at upper mantle pressures and temperatures, (In prep.).

WADE K. and BANISTER A. J. (1973) The chemistry of aluminium, gallium, indium and thallium. In *Comprehensive Inorganic Chemistry,* Vol. 12, pp. 993–1064 Pergamon Press.

WALTER L. S. and DOAN A. S. (1969) A determination of oxygen fugacities of chondritic meteorites (abstr.). *Geol. Soc. Amer. Abstr. Prog.* **1,** 232–233.

WELHAN J. A. and CRAIG H. (1979) Methane and hydrogen in East Pacific Rise hydrothermal fluids. *Geophys. Res. Lett.* **6,** 829–831.

WELHAN J. A. and CRAIG H. (1983) Methane, hydrogen and helium in hydrothermal fluids at 21°N on the East Pacific Rise. In *Hydrothermal Processes at Seafloor Spreading Centers,* (eds. P. A. RONA, K. BOSTROM, L. LAUBIER and K. L. SMITH), pp. 391–409 Plenum Press.

WELTNER W. and MCLEOD D. (1964) Spectroscopy of silicon carbide and silicon vapor trapped in neon and argon matrices at 4 K and 20 K. *J. Chem. Phys.* **41,** 235–245.

WINDOM K. E. and BOETTCHER A. L. (1981) Phase relations for the joins jadeite-enstatite and jadeite-forsterite at 28 kb and their bearing on basalt genesis. *Amer. J. Sci.* **281,** 335–351.

WOERMANN E. and ROSENHAUER M. (1985) Fluid phases and the redox state of the Earth's mantle; extrapolations based on experimental, phase-theoretical and petrological data. *Fortschr. Mineral.* **63,** 263–349.

YASAITIS J. A. and KAPLOW R. (1972) Structure of amorphous silicon monoxide. *J. Appl. Phys.* **43,** 995–1000.

YODER H. S. JR. (1964) Soda melilite. *Carnegie Inst. Wash. Yearb.* **63,** 86–89.

YODER H. S. JR. and TILLEY C. E. (1962) Origin of basalt magma: an experimental study of natural and synthetic rock systems. *J. Petrol.* **3,** 342–532.

APPENDIX

Experimental results along the join $Ne_{55}Fo_{45}$–Ne_{55}–O_{45} P = 28 kbar

Run number	Fo Weight percent	Duration (min.)	T (°C)	Approx. % Cryst.	Products*
VOLATILE-ABSENT					
T-1210**	25	15	1440	40	Fo, Opx, Liq, Qx
T-1213**	25	10	1500	—	Liq, Qx
T-1215**	25	10	1475	30	Fo, Opx, Liq, Qx
T-1218**	25	12	1490	10	Fo, Liq, Qx
H_2O–SATURATED (~30 Weight percent H_2O added as liquid)					
T-1175	18	60	1100	5–10	Fo, Opx, Liq, Qx
T-1237	14	60	1040	20	Opx, Liq, Qx
T-1304	20	60	1100	5	Fo, Liq, Qx
T-1305	16	60	1060	10	Opx, Liq, Qx
CO_2–SATURATED (~15 Weight percent CO_2 generated from $Ag_2C_2O_4$)					
T-1226	30	12	1390	10	Opx, Liq, Qx
T-1227†	35	12	1390	—	Fo, Opx, Liq, Qx
T-1334	37	12	1400	<2	Fo, Liq, Qx, Qcarb
C-H FLUID—SATURATED (~7 Weight percent CH_4 generated from $Al(OH)_3/Al_4C_3$ mix)					
T-1174	18	25	1280	25	Opx, Liq, Qx, Fo (tr)
T-1208	25	20	1350	30	Fo, Opx, Liq, Qx
T-1284	22	20	1380	20	Fo, Opx, Liq, Qx
T-1289††	20	25	1380	10	Opx, Liq, Qx
T-1291	20	25	1360	20	Opx, Fo, Liq, Qx
T-1315	22	30	1395	5	Fo, Liq, Qx

* Fo = forsterite; Opx = enstatite s.s.; Liq = glass; Qx = quench crystals; Qcarb = quench carbonate; tr = trace.
† Liquid composition obtained (see below).
†† FTIR spectrum and difference spectrum obtained (see Figure 7)

Liquid Compositions (Weight percent)

Oxide	T-1213	T-1218	T-1215	T-1210	T-1227*
SiO_2	54.01	54.39	54.55	54.52	48.81
Al_2O_3	19.85	21.51	22.79	23.19	22.93
MgO	14.28	11.03	8.81	8.19	14.32
Na_2O	11.86	13.07	13.85	14.10	13.94
Fe	24.9 (25)†	19.3	15.4	14.3	25.0
Ne	55.3 (55)	59.9	63.5	68.6	63.9
Q	19.8 (20)	20.8	21.1	21.1	11.1

* Liquid projected back into Na/Al = 1 plane from average quench pyroxene: $En_{55}MgTs_{30}Jd_{15}$ (mol percent).
† Expected composition in brackets.